

Experimental Study of Formation Alignment of Multiple Autonomous Air-levitated Vehicles with Rule-based Controls

P.K.C. Wang and J. Yee
Department of Electrical Engineering
University of California
Los Angeles, CA 90024-1594

F.Y. Hadaegh and K. Lau
Jet Propulsion Laboratory
California Institute of Technology
Pasadena, CA 91109-8099

An experimental study is made on the alignment of three autonomous air-levitated vehicles with air-jet controls to achieve an equilateral-triangle formation. The vehicles are equipped with optical sensors, lasers, radio transceivers, and on-board power sources. The attitude and displacement of each vehicle are controlled by air-jets. The main objective is to determine the feasibility of using control rules derived by making use of the sensor data only for formation alignment. The sensors consist of discrete, binary optical detectors arranged in a certain geometric pattern. The vehicle design, including estimation of levitation life-time, sensor design, and vehicle excursion due to an air-jet pulse, are discussed first. Then the control rules are described in detail. The effectiveness of the proposed sensor-control combination in formation alignment is determined both experimentally and via computer simulation.

INTRODUCTION

Recent interest in formation flying of multiple spacecraft and space robots led to a number of studies in the coordination and control of multiple autonomous spacecraft and space robots¹⁻⁶. So far, these studies only considered the feasibility of formation flying for specific applications, the development of control laws and the determination of their effectiveness via computer simulation. Here, we present the results of an experimental study of formation alignment of three air-levitated vehicles equipped with air-jets and special optical sensors

for control. To simulate the space environment in the laboratory, it is necessary to levitate the vehicles. The main objective is to determine the feasibility of using control derived by making use of the sensor data only for formation alignment. No mathematical models for the vehicle dynamics are used in the development of control rules. The sensors consist of discrete, optical detectors with binary outputs. They are arranged in a certain geometric pattern for formation alignment.

The use of large air-levitated multi-arm mobile robots for performing certain tasks such as target rendez-vous and capture has been studied earlier^{7,8}. Here, emphasis is placed on the formation alignment of multiple air-levitated mini-vehicles. These vehicles are not required to perform other tasks.

The paper begins with a description of the experiment. Then the design of air-levitated vehicles is discussed in detail. This is followed by a description of control rules. The dynamic behavior of the vehicles with the derived rule-based controls is studied via computer simulation using a simplified dynamic model. Finally, the experimental results and the effectiveness of the proposed sensor-control combination in formation alignment are discussed.

DESCRIPTION OF THE EXPERIMENT

The experiment involves three autonomous air-levitated vehicles, one of which serves as the *reference vehicle* or *leader* for the remaining vehicles (referred hereafter as *followers*). It is required that the vehicles attain an equilateral-triangle formation in a self-organizing manner without the intervention of external agents. This type of formation is of particular interest in the development of space interferometers with long base lines⁹. In this experiment, the interaction between the vehicles is achieved through laser and optical sensors along with radio transceivers, but it does not involve distance metrology. Thus the size of the triangular formation is not specified. The main reason for not including distance metrology in the

vehicles is the lack of sensors for short distance (< 1 meter) measurement with accuracy better than 1 mm. Figure 1 shows a sketch of three vehicles to be aligned into an equilateral-triangle formation. Each vehicle is equipped with a laser and an optical sensor-module whose axes intersect at an angle of 60 degrees.

The formation-alignment scenario is as follows:

First, the Leader initiates the formation alignment by activating its laser, and rotating about its vertical body-axis to search for Follower 1. When the optical sensors of Follower 1 detect the laser beam, an acknowledgment of the interception is sent to the Leader via radio to terminate the search. Then Follower 1 performs fine alignment of its attitude relative to the direction set forth by the laser beam of the Leader. When this task is completed, the first follower activates its laser, and sends out a radio signal to Follower 2 to initiate the search for the laser beam of Follower 1. This search involves a sequence of prescribed rotational and translational maneuvers. Follower 2 terminates its search as soon as its sensors detect the laser beam of Follower 1. Subsequently, Follower 2 performs a fine alignment of its attitude relative to the direction set forth by the laser beam of Follower 1. Upon completion, it activates its laser. The final alignment step involves the translation of Follower 2 along the direction of the laser beam of Follower 1. The formation alignment is complete when the laser beam of Follower 2 intercepts the sensor of the Leader. An acknowledgment of this interception is sent to Follower 2 by the Leader via radio.

VEHICLE DESIGN

The air-levitated vehicle consists of two modules as shown in Fig.2. The bottom module is an air-filled cavity (pressurized to about 6.2×10^6 dynes/cm² or 90 psi) with a valve-controlled orifice. The outflowing air provides a bearing between the vehicle bottom and a flat surface. The top module is also a pressurized-air cavity with six valve-activated jets for controlling the translational and rotational motions of the vehicle. This cavity has six

compartments interconnected by orifices which serve as baffles during valve activation. The sensor-module, laser, radio transceiver, and micro-controller are mounted above the top module. They are powered by on-board batteries. Provision is made for connection to an external power source during testing without levitation.

Levitation Life Time

Since the vehicles are levitated by an on-board air supply, it is of importance to estimate the length of time over which the vehicle remains levitated above a specified height from the flat surface so that formation-alignment experiments can be performed without interruption.

To simplify the analysis, we introduce the following assumptions: (i) the vehicle is stationary, and its center of mass is along the vertical body-axis passing through the center of the vehicle's circular base; (ii) the mass distribution is symmetric about the vertical axis, and the vehicle's bottom surface is parallel to the ground plane; and (iii) the air-flow out of the vehicle base is isothermal, quasi-steady, axially symmetric and uniform in all radial directions.

Let V and β denote respectively the volume of the bottom cavity and the bulk modulus of air; p_c and p_1 the air pressures inside the small cavity and in the region immediately outside the central orifice respectively. Taking into account the compressibility of air inside the bottom cavity, we have

$$\frac{V}{\beta} \frac{dp_c}{dt} = -\frac{C_{do} A_o C}{\sqrt{T}} (p_c - p_1), \quad (1)$$

where C_{do} and A_o are the discharge coefficient and the area of the central orifice respectively; T the air temperature inside the bottom cavity in °R; and C is a coefficient defined by

$$C = g \sqrt{\frac{k}{R} \left(\frac{2}{k+1} \right)^{\frac{k+1}{k}}}, \quad (2)$$

where k is the ratio of specific heats for air; g the acceleration due to gravity; and R the gas constant.

Let $h(t)$ denote the gap between the vehicle's bottom cavity and the ground plane at time t ; r_O and r_I the radii of the base and the inner cavity respectively (see Fig.3). When $h(t)$ is small compared to $r_O - r_I$ so that the air in the region $\Omega(t) = \{(x, y) : r_I < \sqrt{x^2 + y^2} < r_O; 0 < z < h(t)\}$ forms a thin film, then the air pressure p in this region is describable by the Reynolds equation¹⁰:

$$\frac{\partial}{\partial x} \left(h^3 \rho \frac{\partial p}{\partial x} \right) + \frac{\partial}{\partial y} \left(h^3 \rho \frac{\partial p}{\partial y} \right) = 12\mu \frac{\partial(\rho h)}{\partial t}, \quad (3)$$

where μ is the viscosity coefficient; ρ the air density; and we have neglected the z -variation of pressure p . Under assumption (iii), ρ is proportional to p . When $|dh(t)/dt|$ is small compared to the speed of air outflow so that the pressure p is quasi-static, (3) reduces to

$$\frac{d}{dr} \left(r \frac{dp^2}{dr} \right) = 0 \quad (4)$$

in cylindrical coordinates. The solution to (4) satisfying the two-point boundary conditions

$$p^2(R_I) = p_1^2, \quad p^2(R_O) = p_a^2 \quad (5)$$

is given by

$$p(r) = p_1 \left\{ 1 - \left[1 - \left(\frac{p_a}{p_1} \right)^2 \right] \frac{\ln(r/R_I)}{\ln(R_O/R_I)} \right\}^{\frac{1}{2}} \quad \text{for } R_I \leq r \leq R_O, \quad (6)$$

where p_a is the ambient air pressure.

Balancing the fluid and gravitational forces, we obtain the following nonlinear algebraic equation for the unknown pressure p_1

$$Mg + \pi R_O^2 p_a = \int_{R_I}^{R_O} 2\pi p_1 \left\{ 1 - \left[1 - \left(\frac{p_a}{p_1} \right)^2 \right] \frac{\ln(r/R_I)}{\ln(R_O/R_I)} \right\}^{\frac{1}{2}} r dr + \pi R_I^2 p_1, \quad (7)$$

where M is the total mass of the vehicle. Due to the quasi-static assumption, this equation is independent of the gap or air-film thickness h . Moreover, (7) is valid only when $h(t) >$

0. Since the integral in (7) cannot be readily evaluated in closed-form, we introduce the following straightline approximation of the pressure distribution $p(r)$ in (6):

$$p(r) \approx p_a + (p_1 - p_a) \frac{(R_O - r)}{(R_O - R_I)}. \quad (8)$$

Figure 4 shows the graphs of p/p_a versus r/R_I for various values of p_1/p_a , and the corresponding straightline approximations. It can be seen that (8) represents a good approximation to $p(r)$. Substituting (8) into (7) leads to the following approximate expression for p_1 :

$$p_1 \approx p_1^* = \frac{3(R_O - R_I)}{\pi(R_O^3 - 3R_O R_I^2 + R_I^3)} (Mg + p_a \pi R_I^2) + p_a \quad \text{for } R_I \leq t \leq R_O, \quad (9)$$

which, in view of (1), gives a differential equation for p_c :

$$\frac{dp_c}{dt} = -(p_c - p_1^*)/\tau_c, \quad (10)$$

where

$$\tau_c \doteq V \sqrt{T}/(\beta C_{do} A_o C). \quad (11)$$

The solution to (10) corresponding to initial condition $p_c(0)$ at $t = 0$ is given by

$$p_c(t) = (p_c(0) - p_1^*) \exp(-t/\tau_c) + p_1^*, \quad t \geq 0. \quad (12)$$

Thus the equilibrium air pressure in the bottom cavity is $p_c^e \approx p_1^*$.

Ideally, the *levitation life-time* should be defined as the time required for the gap h to drop down to a specified level. However, due to the quasi-static approximation, the foregoing results are independent of h . Therefore, we define levitation life-time t_{lev} as the time required for the pressure difference $(p_c - p_1^*)$ to drop down to $\alpha(p_c(0) - p_1^*)$, where α is a specified positive number < 1 . Thus, we have $t_{lev} = -\tau_c \ln \alpha$ which only depends only on the parameters of the central orifice.

Optical Sensor Module

The design of the optical sensor module is crucial to the development of rule-based control laws for formation alignment based on simple geometric ideas. The optical sensor module not only detects the interception of the laser beam emanated from other vehicles, it also provides information on the attitude of the vehicle relative to the incoming laser beam direction. Fig. 5a shows the optical sensor module which consists of an optically transparent post with a polygonal cross-section, and a single thin solar-cell located at the center of sensor module. One edge of the polygon is shorter than the remaining ones. The short edge provides a narrow window to allow laser-beam activation of the central cell. The outputs of the cells are fed into a comparator with the other input set to a variable voltage which is adjusted to cancel the effect of ambient light. Thus the outputs of the sensor module are binary. The height of the sensor module is adjustable so that it can be set to sense the laser beam emanated from a particular vehicle only.

For this experiment, the sensor module has only five cells. The central cell (labelled "C") is 0.159×1 cm in size, and has a planar aperture of 24.24 degrees. Each of the remaining cells (labelled by "RF" (right front), "RR" (right rear), "LF" (left front), and "LR" (left rear)) is 0.5×2 cm in size. Fig. 5b shows a photograph of the actual sensor module.

Actuator/controller Unit

The translational and rotational motions of the vehicle are controlled by six air-jets arranged in a "H-pattern" as shown in Fig.6. The jets are labelled "RF" (right front), "R" (right), "RR" (right rear), "LR" (left rear), "L" (left), and "LF" (left front), and they are controlled by electromagnetic valves. The valve activation and deactivation time-delays are approximately 4-5 milliseconds with negligible hysteresis. For forward (resp. backward) translational motion, the LR and LF (resp. RF and LF) jets are activated. For side motion, only the R or L jet is activated.

In the present experiment, the valves are operated in a pulsed mode with fixed duration in the range of 15–50 milliseconds. In the ideal frictionless case where the vehicle has only pure inertia, it is also necessary to activate the air jets in the direction of motion to stop the vehicle. Since friction exists in the air-bearing formed by the vehicle base and the flat surface, we make use of this friction to stop the vehicle after each air-jet pulse. Thus, each vehicle moves in a stepwise manner. The step size is estimated by the following simplified analysis.

Consider a single air-jet with orifice area A_J and discharge coefficient C_{dJ} . Assuming that the flow is choked, the average velocity v_J of the air-jet is given by

$$v_J = C_{dJ} C p_u / (g \rho \sqrt{T}), \quad (13)$$

where C is a coefficient defined in (2), and p_u is the air pressure (gauge) inside the top cavity. When the duration τ_p of the valve opening is long compared to the activation and deactivation time-delays of the valve, the impulse or thrust F produced by the air-jet pulse is given by $F = \rho A_J v_J^2$. Thus from the change of linear momentum of the vehicle, the increment in vehicle velocity at the end of the air-jet pulse with duration τ_p is given by

$$\Delta v = \rho A_J v_J^2 \tau_p / M, \quad (14)$$

where the vehicle is assumed to be at rest initially. For $t > \tau_p$, the vehicle motion satisfies

$$M dv/dt + \nu v = 0, \quad (15)$$

where ν is a positive friction coefficient. Solving the above equation with initial condition (14) and zero displacement at the end of the air-jet pulse $t = \tau_p$, we obtain the vehicle displacement

$$s(t) = (M \nu \Delta v) (1 - \exp\{-\nu(t - \tau_p)/M\}) \quad \text{for } t \geq \tau_p. \quad (16)$$

Thus the steady-state displacement $s_{ss} = \lim_{t \rightarrow \infty} s(t)$ is given explicitly by

$$s_{ss} = \frac{A_J \tau_p C_{dJ}^2 P_u^2}{\rho T \nu} \left\{ \frac{k}{R} \left(\frac{2}{k+1} \right)^{\frac{k+1}{k-1}} \right\}. \quad (17)$$

Evidently, s_{ss} is inversely proportional to the friction coefficient ν whose value can be determined experimentally.

Following the same approach, it can be verified that the steady-state angular displacement ϕ_{ss} for the vehicle about its vertical body axis due to a pulsed air-jet couple is given by

$$\phi_{ss} = 2r_a s_{ss} \nu / \hat{\nu}, \quad (18)$$

where $\hat{\nu}$ denotes the friction coefficient for the rotational motion, and r_a the perpendicular distance between the air-jet axis and the vehicle's vertical body axis.

RULE-BASED CONTROLS

The development of control rules is based on simple geometric ideas. Fundamental to this approach is to use a small number of optical sensors at prescribed locations such that their outputs provide sufficient information for formation alignment. Here, the information on the dynamics of the vehicle is embedded in the sensor output data (present and past values).

The air valves are activated by signals generated by a rule-based controller. Moreover, the valves operate in a pulse mode, and the vehicle moves in a stepwise manner. The basic motion commands are: CR (clockwise rotation), CCR (counterclockwise rotation), FT (forward translation), BT (backward translation), RT (right translation), LT (left translation), and S (stop). The correspondence between the motion command and valve activation is shown in Table 1.

From the formation-alignment scenario described earlier, it is clear that the control rules for the Leader are different from those for the Followers. Moreover, the control rules consist

of a mixture of open-loop and closed-loop commands. The method used to bring a vehicle, either Follower 1 or Follower 2, into alignment with a laser beam relies on a combination of the physical sensor configuration and the underlying software algorithm. An enabling factor which allows the vehicle to be aligned with a laser beam is the presence of an aligning element within the sensor configuration. While seemingly obvious, the presence of such an element need not be a physical part of the sensor, merely a consequence of the sensor geometry. Sensor geometry also plays a large role in determining the nature of the underlying algorithm. Without exact knowledge of the nature of the sensors available and how they are arranged, it is difficult to state a clear algorithm for formation alignment. A novel sensor geometry can vastly simplify the underlying algorithm.

The aligning element in our present experiment is a central sensor embedded in an optically transparent post with pentagonal cross-section as described earlier. The central sensor has a very narrow viewing window which is crucial to the alignment task.

The control algorithm was designed with several factors in mind. One was that since all the energy sources including the batteries and compressed air sources are onboard, the algorithm should be fuel efficient by avoiding unnecessary maneuvers. Another was that due to limited precision of the hardware components, and variations in air friction, a maneuver was not exactly reproducible or reversible. For instance, a clockwise rotation produced by a given finite sequence of valve pulsations is not exactly undone by a counter-clockwise rotation of the same sequence of valve pulsations. Thus, our control algorithm does not rely upon performing a number of tentative maneuvers to ascertain what must be done before doing it. Rather, it proceeds in a surefooted manner, making the proper decisions as events warrant, never backtracking to regain an initial position.

The overall operation of our control algorithm is as follows. Each of the three vehicles has a laser and a sensor array which basically looks in all directions for a laser beam. The

viewing direction of the central sensor and the laser beam of each vehicle are fixed at 60° with respect to each other. Thus the final positions of the vehicles form an equilateral triangle. As there is no metrology and all equilateral triangles are similar, an equilateral triangle with sides approximately equal to the initial distance between the Leader and Follower 1 is all that can be guaranteed. The Leader initiates a search by turning on its laser and performing an in-place rotation, scanning the laser beam, all the while waiting for a radio signal from Follower 1 acknowledging beam acquisition. Upon the reception of the radio signal from Follower 1, the Leader immediately stops its rotation and holds the beam steady.

Follower 1 performs a sequence of maneuvers based on which sensor was initially hit and subsequent sensor hits. These maneuvers end when the central sensor of Follower 1 is looking at the laser beam from the Leader. Thus, the Leader and Follower 1 are aligned. Follower 1 then turns on its own laser and sends a radio signal to Follower 2, telling it to begin its search for the laser beam.

Follower 2, activated by the radio signal from Follower 1, initiates a preprogrammed search for the laser beam from Follower 1. Once acquired, Follower 2 uses the same algorithm as Follower 1 to center itself on the beam, ending with its central sensor looking at the beam from Follower 1 through a narrow slot. At this point, Follower 2 turns on its laser and maneuvers straight back and forth along the beam of from Follower 1, waiting for a radio signal from the Leader to stop its search. Since the angle between the laser and the central sensor on each vehicle is fixed, the final result is an equilateral triangle with the vehicles at the vertices, and the laser beam from each vehicle forming the sides. The algorithm terminates.

A flow chart for the control algorithm is shown in Fig. 7. It can be seen that the algorithm possesses six main branches to reflect the presence of five sensors and the possibility that none of the sensors is activated. The latter is due either to the sensor array not being in

line with the laser beam or the window for central sensor C being in line, but the underlying sensor is rotationally offset. For this sensor configuration, we designed the vehicle to rotate about the viewing window of the central sensor rather than the seemingly more natural choice of rotating about the central vertical axis of the sensor.

If the vehicle is almost aligned such that the LF and RF sensors are alternately illuminated during the maneuver, we can conclude that the vehicle is close to alignment except for a slight rotation. However, due to the geometry of the viewing slot of sensor C, there exists a gap in the sensor viewing angles where the window of sensor C is illuminated by the laser beam but not sensor C itself. In this case, our algorithm calls for centering on the blind spot of the sensor C window, and then uses it as the center of rotation to swing sensor C into the beam. Had the vehicle been constructed with sensor C rather than its window as the center of rotation, this terminal maneuver would not have been so easily accomplished.

Returning to the flow chart, the cluttered appearance can be rectified somewhat by realizing that physical symmetries in the vehicle appear as symmetries in the algorithm. Thus, the branches handling the front sensors LF and RF are almost mirror images of each other with the roles of LR and RR reversed, as well as LF and RF. The reflection axis being the central vertical axis of the vehicle. Similarly, the branches handling the rear sensors LR and RR, also share the same mirror image relationship. The branch to handle the absence of sensor readings also exhibits internal symmetry.

In operation, the algorithm basically remembers the first sensor that was hit, and then uses it along with the currently activated sensor to make decisions. Unless the terminal subroutines (TAIL or FINE alignment subroutine) are called, the program repeatedly executes the sequence:

Loop

Which sensor is hit?

Which sensor was hit initially?

Perform action

If not in TAIL or FINE, go to Loop

The control rules can also be expressed in the form of IF-THEN statements. Let the sensor-module output of the i -th vehicle at any time t is represented by an ordered quintuple $w_i(t) = (w_{i1}(t), \dots, w_{i5}(t))$, where $w_{ij}(t) = 1$ or 0 , $j = 1, \dots, 5$, $i = 0, 1, 2$, the subscript $i = 0$ denotes the Leader. Since the height of the sensor-module is set to sense the laser beam from a particular vehicle only, $w_i(t)$ can have at most one nonzero component.

The Leader and Follower 2 are each equipped with a radio receiver and transmitter whose states are denoted respectively by binary-valued variables RV_i and TX_i , $i = 0, 2$ (i.e. $RV_i = 1$ when a signal is received, and $RV_i = 0$ otherwise). By using suitable decoders, the receiver of the Leader is restricted to receive coded signals from Follower 1 only, while the receiver of Follower 2 is restricted to receive coded signals from the Leader only. Follower 1 has a pair of transmitters for sending coded signals to the Leader and Follower 2. Their states are denoted by binary-valued variables TX_{11} and TX_{12} . Follower 2 has two radio receivers whose states are denoted respectively by binary-valued variables RV_{21} and RV_{22} . Finally, the state of the laser for the i -th vehicle is denoted by the binary-valued variable LA_i , $i = 0, 1, 2$, where $LA_i = 1$ for laser ON, and $LA_i = 0$ for laser OFF.

Using the foregoing variables, we can express the control rules for the vehicles in the form of IF-THEN statements. For example, the control rules for the Leader can be stated as:

1. If $RV_0 = 0$ AND $w_0 = 0$, then set $LA_0 = 1$ and MOTION COMMAND = CR for a preset number of time steps, followed by MOTION COMMAND = CCR for a preset number of time steps.
2. If $RV_0 = 1$, then set MOTION COMMAND = S.

3. If $RV_0 = 1$ AND $w_0 \neq 0$, then set $TX_0 = 1$.

The control rules for the FINE alignment subroutine depend on both the present and past value of the sensor output. These rules can also be expressed in the form of IF-THEN statements. In the experimental vehicles, the rule-based controls are implemented in assembly language on the Miniboard, a small controller board developed by Martin at MIT, using the Motorola 68HC11 mpu.

Fundamental to our control algorithm is a detailed partitioning of the set of all direction angles ($[0^\circ, 360^\circ]$) at which a vehicle with an activated laser beam could appear with respect to the sensor of another vehicle. Since the sensor has essentially a square shape, there are four distinct groups of partitions. The derivation of the partitions is somewhat tedious. To illustrate the basic ideas, we give the complete partitioning scheme for the case where the RR (right-rear) sensor of Vehicle A is hit initially by the laser beam from Vehicle B.

Our control algorithm is based on the fact that information pertaining to the relative attitude of the vehicles can be acquired through vehicle motion. We chose an initial rule that compels movement towards the right (looking out from the central sensor C of Vehicle A) when the RR sensor of Vehicle A is initially hit by the laser beam from Vehicle B. Figure 8 shows the angular relationship between the incoming beam QP and the axis CT of the central sensor C, and how this relationship can be inferred from the sensor activation history.

In the upper-left figure, the rightward movement (as indicated by the small arrow) after an initial hit on the RR sensor eventually leads to loss of sensor contact with the laser beam if the angle $\hat{\theta}$ between the laser beam and the sensor axis lies in the interval $\hat{I} = [-135^\circ, -90^\circ]$. To provide better understanding of the sketches in Fig.8, we show cases where $\hat{\theta}$ is offset slightly from the end points of \hat{I} . In these and all intermediate cases, vehicle movement in the direction of the small arrow eventually walks the laser beam off the RR sensor, and results in a loss of sensor contact with the laser beam. The information thus inferred is that

the angular position of the Vehicle B relative to Vehicle A lies somewhere in the interval \hat{I} .

The upper-right figure shows the exceptional case where the sensor axis CT is perpendicular to the laser beam QP . Rightward movement, as stipulated by our rule, does not lead to change in the sensor readings. By including a timeout depending on the sensor size and strength of the control jets, we escape an endless loop and infer that the angular position of Vehicle B is -90° relative to Vehicle A.

The lower-left figure shows the borderline cases for rightward movement in which the laser beam from Vehicle B hits the RR sensor of Vehicle A initially, and then hits the RF sensor after some rightward movement by Vehicle A. For this sequence of events, we infer that Vehicle B lies on a minor arc subtended by angles -90° and -45° .

Finally, in the lower-right figure, the laser beam from Vehicle B initially hits the RR sensor of Vehicle A and subsequently hits the LR sensor after a rightward movement. This case implies that Vehicle B lies on a minor arc subtended by angles -135° and 135° . The union of all the partitions is a flat angle of 180° as in the case of a flat sensor panel. Other partitions can be derived in a similar way. They are given in Fig.9.

The numerical values for the angles shown in Fig.9 indicate the laser beam angle relative to the axis of the central sensor, where 0° implies alignment. Listed within the angular sectors are the sequence of sensor events leading to the conclusion of the indicated angle. The italic letters indicate the action taken by the vehicle once the relative angle has been determined. The actions corresponding to initial laser-beam hits on the LF and RF sensors should result in the eventual takeover by the FINE subroutine which leads to alignment. The indicated actions for the initial hits on LR and RR sensors should result in forward sensor impingement. The TAIL subroutine, with a bias in the initial search direction, should result in quick entry into the FINE subroutine and subsequent alignment.

To clarify the vehicle maneuvers generated by the control algorithm, we consider a partic-

ular scenario where the laser beam from the Leader initially hits the RR sensor of Follower 1 as shown in the top sketch of Fig.10. Our alignment scheme calls for Follower 1 to send a radio signal to the Leader to stop its search, followed by an initial rightward movement of Follower 1 as indicated by the small arrow. When the LR sensor of Follower 1 is hit by the beam, we infer that the Leader lies within the right angle $[-135^\circ, 135^\circ]$, or in short, the Leader is somewhere behind Follower 1. Our rule is to execute a 180° turn. Due to the fact that the center of rotation is set at the a point on the window of the central sensor C, Follower 1 loses contact with the laser beam as shown in the third sketch in Fig.10. Despite this loss, we know that the beam is at the front side of Follower 1, but shifted slightly to one side. Under this condition, the TAIL subroutine takes over, and executes a short search for the beam by moving the vehicle to the right and left for a prescribed number of steps, and then turns over control to the FINE subroutine once the beam is located. In the FINE subroutine, Follower 1 moves right or left, if the beam hits the RF or LF sensor respectively. This translational motion leads to interception of the beam with the window of the central sensor C. Subsequently, the subroutine calls for a rotation of Follower 1 about the point of interception so that Follower 1 is aligned with the laser beam of the Leader as depicted by the last sketch of Fig.10. Now, Follower 1 turns on its laser beam, and signals Follower 2 via radio to commence its search for the beam. Follower 2 uses the same beam alignment procedure for Follower 1 when the beam hits any sensor of Follower 2. Once the alignment is attained, we have the situation that the Leader's beam forms one side of a triangular formation, while Follower 2 lies along a ray \mathcal{R} which is at a 60° angle from the Leader's beam. At this point, Follower 2 turns on its laser beam which is at a 60° angle from the beam from Follower 1. Since we do not wish to lose beam contact between Followers 1 and 2, the search for the Leader by Follower 2 is restricted to moving forward and backwards along the ray \mathcal{R} while waiting for a radio signal from the Leader acknowledging the beam

contact. This forward-backward motion is accomplished by keeping the FINE subroutine active during the maneuver. The FINE subroutine uses only the Left and Right air-jets to keep the laser beam from Follower 1 fixed on the central sensor of Follower 2. Finally, the triangular formation alignment terminates when the central sensor of the Leader is hit by the laser beam from Follower 2.

Table 2 shows a summary of the algorithm's actions corresponding to initial laser-beam hits on each of the four sensors LF, RF, RR and LR. This table was made during algorithm development to ensure that all possibilities were accounted for. The angle attached to the end of each arrow indicates the angle which the laser beam makes with the horizontal axis of the central sensor (0° indicates alignment). Thus, an initial hit on the central sensor C would signify an already perfect alignment. The sequence of sensor events leading to the inference of the corresponding angular range is shown inside the angular sector for that range. For instance, the lower right diagram is for an initial hit on the RR (right-rear) sensor, and the sensor sequence "RR,LR" indicates that the subsequent maneuver caused the LR (left-rear) sensor to be hit, thus leading to the inference that the laser-beam angle is within the interval $[-135^\circ, 135^\circ]$, and calling for a clockwise turn of 180° as indicated by the notation in italic letters. If all the sensor readings go to zero after moving right, we have the sequence "RR,0", indicating that the vehicle is facing the $(-90^\circ, -135^\circ)$ arc and a clockwise rotation of 90° is called for. If the sensor readings do not change and a timeout is reached, the front of the vehicle is very close to being perpendicular to the beam, so again, a 90° rotation is needed. Finally, if the RR sensor is illuminated first, and rightward movement brings the RF sensor into the laser beam, the sensor sequence is "RR,RF", implying that the vehicle is facing the $(-45^\circ, -90^\circ)$ arc. In this case, a 45° clockwise rotation is performed. After this sequence, the TAIL and FINE subroutines take over.

Table 2 also summarizes the algorithm in another way. Reading from left to right, the

sequence of actions and inferences at each step can be found. The scenario described earlier can be easily followed on the table. This table summarizes the algorithm in a manner akin to a decision tree, while Fig. 9 summarizes it geometrically.

COMPUTER SIMULATION STUDY

To determine the effectiveness of the rule-based controls described in the last section, computer simulation studies are made using a simplified dynamic model for the vehicles described in Appendix A. Here, the laser beam is assumed to be a line with zero cross-section so that the task of determining which sensor element is being hit by the beam can be simplified (see Appendix A). In what follows, we only present the simulation results for alignment between the Leader and Follower 1 for the scenario described in the previous section. Figure 11a shows the time-domain behavior of the angular positions of the Leader and Follower 1 during their alignment period. The vehicles start from rest at $(x_0(0), y_0(0)) = (0, 50)$ and $(x_1(0), y_1(0)) = (35, 0)$ cm with initial attitude angles $\theta_0 = 5.74, \theta_1 = 3\pi/2$ rad. It can be seen from Fig. 11a that the Leader starts rotation at $t = 0$, and its laser beam intercepts the sensor of Follower 1 at $t = 12.35$ sec. and the Leader stops its rotation. Since the laser beam hits the RR sensor of Follower 1, the control algorithm initiates a translational maneuver until the laser beam intercepts the LR sensor of Follower 1 at $t = 16$ sec. At this time, Follower 1 initiates a 180° clockwise rotation, and stops at $t = 31.75$ sec. Since the laser beam hits the central sensor C after the rotation, no further alignment maneuver is necessary. To check the robustness of the control algorithm with respect to disturbances, we repeat the foregoing simulation except at the end of 180° rotation, an instantaneous 1-cm perturbation in the position of Follower 1 along the x -direction is introduced. This displacement offset causes a loss of contact with the Leader's laser beam, and activates the TAIL alignment subroutine to initiate a sideway translational search for the beam. It

can be seen from Fig.11b that the search terminates at 36.9 sec. when the beam hits the central sensor C. Note that in this case, the perturbation induces a $2.75\text{-}\mu\text{m}$ displacement of Follower 1 in the y -direction. However, this displacement does not affect the final alignment. Similar results can be obtained for the alignment between Followers 1 and 2, and between Follower 2 and the Leader.

EXPERIMENTAL RESULTS

Figure 12 shows a photograph of the experimental setup consisting of three air-levitated vehicles on a granite surface with flatness within $10\mu\text{m}$. Each vehicle was carefully balanced so that the planar locations of the center of mass and the window of the central sensor coincide. It was observed that the levitated vehicle is highly sensitive to offsets in the level of the granite surface, and air disturbance. The parameter values of the actual vehicle are given in Appendix B.

In the experiment, the initial task was to determine the levitation life-time experimentally. This was accomplished by attaching a small pressure gauge to the inlet of the bottom cavity, and observing the pressure decay as a function of time. The experimental result shown in Fig. 13 is consistent with that obtained analytically.

Next, we varied the width of the voltage-pulse to the valve drivers by observing the resulting movement of the laser-beam spot on a flat surface. Since the minimum effective pulse-width for valve activation is of the order of 15 msec, and the air friction is small initially and increases as the vehicle body descends towards the surface, it was necessary to introduce an additional short-duration pulse to the opposing valves to produce the reverse torque or force pulse to stop the vehicle motion. Moreover, the pulse duration is progressively lengthened to compensate for the effect of air depletion in the top cavity resulting from control-jet activation.

Finally, we activated the control and sensor modules of all the vehicles, and observed their dynamic behavior in self-organization. Due to the small size (122×92 cm) of the granite surface, tests were made with initial vehicle separation distance ≤ 60 cm. Since the levitation life-time is of the order of 4 minutes, experimental test runs were limited to small rotational and translational maneuvers. Equilateral triangular formation was attained when the initial formation of the vehicles was near the desired one. The formation alignment motions were recorded by means of a video camera. However, it was impossible to obtain meaningful hardcopy records since the formation alignment motions were minute, and no distance or angular-position sensors were used in this experiment.

CONCLUSION

We have demonstrated experimentally that formation alignment for multiple air-levitated vehicles can be attained by using rule-based controls activated by discrete optical sensors arranged in a simple geometric pattern. One may consider other sensor patterns that lead to different rule-based controls. In this experiment, since both the sensor outputs and actuator inputs are binary valued, it is natural to use classical logic for rule-based controls. The proposed approach of using a special sensor-control combination for formation alignment may also be applicable to real spacecraft and free-flying space-robots using small micro-controllers.

In this experiment, no distance metrology is used because of the lack of available accurate sensors for short distance measurement. For experiments involving triangular formations with dimensions greater than 10 meters, it is possible to incorporate available distance sensors into the vehicles so that formations with specified dimensions can be attained.

Although in this experiment, the vehicle is restricted to planar motions, some of the ideas presented here can be extended to the 3-D case by considering 2-D projections of the formation patterns in 3-D space. However, a laboratory experiment for 3-D motions requires a levitation scheme which differs from the one used here. Finally, future experiments will involve a large number of sensors arranged in various geometric patterns to obtain more fuel-efficient controls for formation alignment.

Acknowledgment

This work was performed under contract No.960570 with the Jet Propulsion Laboratory, California Institute of Technology, Pasadena, California. The authors wish to thank the referees for their careful reviews and helpful comments.

References

1. R. Stachnik, R. Melroy and D. Arnold, "Multiple spacecraft Michelson stellar interferometry," *Proc. SPIE, Instrumentation in Astronomy V*, **445**, 358-369 (1984).
2. P.K.C. Wang, "Interaction dynamics of multiple autonomous mobile robots with simple navigation strategies," *J. Robotic Systems* **6**, 77-101 (1989).
3. D. Miller, "Multiple behavior-controlled micro-robots for planetary surface missions," *Proc. IEEE Systems, Man, and Cybernetics Conf.* Studio City, CA, (1990).
4. A.B. DeCue, "Multiple spacecraft optical interferometry, preliminary feasibility assessment," JPL Tech. Internal Rpt. D-8811, August (1991).
5. P. K. C. Wang, "Navigation strategies for multiple autonomous mobile robots moving in formation," *J. Robotic Systems* **8**, 177-195 (1991).
6. P. K. C. Wang and F. Y. Hadaegh, "Coordination and control of multiple microspacecraft moving in formation," *J. Astronautical Sciences*, **44**, 315-355 (1996).
7. M.A. Ullman, "Experiments in autonomous navigation and control of multi-manipulator free-flying space robots," Ph.D. Thesis, Stanford Univ. March, (1993).
8. K.R. Zimmerman and R.H. Cannon, Jr. "Experimental demonstration of GPS for Rendezvous between two prototype space vehicles," *Proc. Inst. of Navigation GPS-95*, Sept. (1995).
9. K. Lau, M. Colavita, and M. Shao, "The new millennium separated spacecraft interferometer," Presented at the Space Technology and Application International Forum (STAIF-97), Albuquerque, NM, Jan. 26-30, 1997.
10. W.E. Langlois, *Slow Viscous Flow*, MacMillan, N.Y. 1964.

APPENDIX A Vehicle Model for Computer Simulation Studies

We use an inertial coordinate system \mathcal{F}_o in the (x, y) -plane with orthonormal basis $\mathcal{B} = \{\mathbf{e}_x, \mathbf{e}_y\}$ as shown in Fig. 14. The representation of the position of the center of mass of the i th vehicle relative to \mathcal{F}_o is specified by $\mathbf{r}_i = x_i\mathbf{e}_x + y_i\mathbf{e}_y$ or the column vector $(x_i, y_i)^T$. Let Δt be a specified sampling time period. Assuming that the air-jets are activated at the beginning of each sampling period $t = k\Delta t$, and that the air-jet pulse duration τ_p is short compared to Δt , the translational motion of the i -th vehicle can be described by the following difference equation corresponding to (15):

$$\mathbf{s}_i(k+1) = \mathbf{H}_i(\Delta t)\mathbf{s}_i(k) + \mathbf{g}_i(\Delta t)\Delta v_i, \quad k = 0, 1, 2, \dots; \quad i = 0, 1, 2, \quad (\text{A-1})$$

where $\mathbf{s}_i(k)$ denotes the column vector $(x_i, \dot{x}_i, y_i, \dot{y}_i)^T$ at time $k(\Delta t)$; and

$$\mathbf{H}_i(\Delta t) = \begin{bmatrix} 1 & \frac{M_i}{\nu}(1 - \exp(-\frac{\nu\Delta t}{M_i})) & 0 & 0 \\ 0 & \exp(-\frac{\nu\Delta t}{M_i}) & 0 & 0 \\ 0 & 0 & 1 & \frac{M_i}{\nu}(1 - \exp(-\frac{\nu\Delta t}{M_i})) \\ 0 & 0 & 0 & \exp(-\frac{\nu\Delta t}{M_i}) \end{bmatrix}, \quad (\text{A-2})$$

$$\mathbf{g}_i(\Delta t) = \begin{bmatrix} \frac{M_i}{\nu}(1 - \exp(-\frac{\nu\Delta t}{M_i})) \cos(\hat{\theta}_i) \\ \exp(-\frac{\nu\Delta t}{M_i}) \cos(\hat{\theta}_i) \\ \frac{M_i}{\nu}(1 - \exp(-\frac{\nu\Delta t}{M_i})) \sin(\hat{\theta}_i) \\ \exp(-\frac{\nu\Delta t}{M_i}) \sin(\hat{\theta}_i) \end{bmatrix}, \quad (\text{A-3})$$

where $\hat{\theta}_i = \tan^{-1}(y_i/x_i)$, $\Delta v_i = \pm 2\Delta v$ when the front or rear control jets are activated; and $\hat{\theta}_i = \tan^{-1}(y_i/x_i) + \pi/2$, $\Delta v_i = \pm \Delta v$ when the right or left control jet is activated, where Δv is given by (14) with M replaced by M_i . The sign of Δv_i depends on which control jet is being activated.

Similarly, the rotational motion of the i -th vehicle about its vertical central axis can be described by the following difference equation:

$$\mathbf{p}_i(k+1) = \mathbf{R}_i(\Delta t)\mathbf{p}_i(k) + \mathbf{s}_i(\Delta t)\Delta \hat{\theta}_i, \quad k = 0, 1, 2, \dots; \quad i = 0, 1, 2, \quad (\text{A-4})$$

where $\mathbf{p}_i(k)$ denotes the column vector $(\theta_i, \dot{\theta}_i)^T$ at time $k(\Delta t)$, and

$$\mathbf{R}_i(\Delta t) = \begin{bmatrix} 1 & \frac{I_i}{\dot{v}}(1 - \exp(-\frac{\dot{v}\Delta t}{I_i})) \\ 0 & \exp(-\frac{\dot{v}\Delta t}{I_i}) \end{bmatrix}, \quad \mathbf{s}_i(\Delta t) = \begin{bmatrix} \frac{I_i}{\dot{v}}(1 - \exp(-\frac{\dot{v}\Delta t}{I_i})) \\ \exp(-\frac{\dot{v}\Delta t}{I_i}) \end{bmatrix}, \quad (A-5)$$

where $\Delta\theta_i = \pm 2r_a\rho A_J v_j^2 \tau_p / I_i$.

Now, we consider the task of determining whether the laser beam from one vehicle hits the sensors of another vehicle; moreover, which sensor is being hit. In our computer simulation study, our algorithm for performing this task is based on the following ideas.

To determine whether any sensor is hit by the incoming laser beam represented by a vector \mathbf{b}_j emanating from \mathbf{r}_j , the center of j -th vehicle (see Fig.15), we introduce the vectors \mathbf{V}_{ik} corresponding to the k -th vertex of the sensor module of the i -th vehicle. These vectors depend on the position \mathbf{r}_i and attitude angle θ_i of the i -th vehicle. Let $\mathbf{w}_{ij}^{(k)} = \mathbf{V}_{ik} - \mathbf{r}_j$. The set of vectors $\mathcal{S} = \{\mathbf{w}_{ij}^{(k)}, k = 1, \dots, 5\}$ defines a cone \mathcal{C} whose aperture angles can be readily determined by computing the minimum and maximum angles associated with \mathcal{S} . Evidently, the laser beam from the j -th vehicle hits the sensor module of the i -th vehicle, if \mathbf{b}_j lies in the cone \mathcal{C} .

To determine which sensor is being hit by the laser beam, we only need to consider those sensors which face the laser beam. This can be determined by introducing unit normal vectors $\mathbf{n}_1, \mathbf{n}_2, \mathbf{n}_3, \mathbf{n}_4, \mathbf{n}_5$ associated with the window lines of sensors C, RF, RR, LR and LF respectively (see Fig.15). If the inner product $\langle \mathbf{n}_k, \mathbf{b}_j / \|\mathbf{b}_j\| \rangle$ is positive, then the k -th sensor is occluded from the laser beam. Thus, the sensors that face the beam can be determined. By considering the cones defined by $\mathbf{w}_{ij}^{(k)}$ associated with the vertices of adjacent sensor pairs facing the beam, we can readily identify which sensor is being hit by the beam.

APPENDIX B Vehicle Parameter Values

V (Volume of bottom cavity): 721 cm^3 .

R_O (Outer radius of bottom cavity): 6.35 cm .

R_I (Radius of bottom cavity indentation): 1.5875 cm .

β (Bulk modulus of air): $6.523 \times 10^8 \text{ dynes/cm}^2$.

C_{do} (Discharge coefficient of central orifice): 1.0 .

A_o (Area of central orifice): $1.237 \times 10^{-3} \text{ cm}^2$.

C (Coefficient defined in (2)): $0.532^\circ \text{ R}^{\frac{1}{2}} / \text{sec}$.

T (Temperature): 529.46° R .

M (Total mass of vehicle): $2.993 \times 10^3 \text{ gm}$.

A_J (Air-jet orifice area): $2.0258 \times 10^{-3} \text{ cm}^2$.

C_{dJ} (Discharge coefficient of air-jet orifice): 1.0 .

Table 1 Motion Command vs Valve Activation

Command	Valve Activation					
	LF	L	LR	RF	R	RR
CR	1	0	0	0	0	1
CCR	0	0	1	1	0	0
FT	0	0	1	0	0	1
BT	1	0	0	1	0	0
RT	0	1	0	0	0	0
LT	0	0	0	0	1	0
S	0	0	0	0	0	0

Initial Hit	Initial Action	Initial Sequence	2nd Hit	2nd Sequence	Inferred Angle	2nd Action	Resulting Angle	3rd Routine
RF	go Right	RF,RF	Nothing	RF,O	[-90,-45]	CW 65	[-25,20]	Fine
			Timeout	RF,RF	-90	CW 90	0	Fine
			C	RF,C	0	to Fine	0	Fine
			LF	RF,LF	[-45,45]	to Fine	[-45,45]	Fine
			LR	RF,LR	Impossible	set LR hit	[45,-135]	LRAct*
			RR	RF,RR	[-135,-90]	CW 110	[-25,20]	Fine
C	All Stop	C,C	C	C,C	0	stay Fine	0	Fine
LF	go Left	LF,LF	Nothing	LF,O	[45,90]	CCW 65	[-20,25]	Fine
			Timeout	LF,LF	90	CCW 90	0	Fine
			C	LF,C	0	to Fine	0	Fine
			RF	LF,RF	[-45,45]	to Fine	[-45,45]	Fine
			LR	LF,LR	[90,135]	CCW 110	[-20,25]	Fine
			RR	LF,RR	Impossible	set RR hit	[135,-45]	RRAct*
LR	go Left	LR,LR	Nothing	LR,O	[90,135]	CCW 110	[-20,25]	Fine
			Timeout	LR,LR	90	CCW 90	0	Fine
			C	LR,C	Impossible	to Fine	0	Fine
			LF	LR,LF	[45,90]	CCW 65	[-20,25]	Fine
			RF	LR,RF	Impossible	set RF hit	[45,-135]	RFAct*
			RR	LR,RR	[135,-135]	CCW 180	[-45,45]	Fine
RR	go Right	RR,RR	Nothing	RR,O	[-135,-90]	CW 110	[-25,20]	Fine
			Timeout	RR,RR	-90	CW 90	0	Fine
			C	RR,C	Impossible	to Fine	0	Fine
			LF	RR,LF	Impossible	set LF hit	[135,-45]	LFAct*
			RF	RR,RF	[-90,-45]	CW 65	[-25,20]	Fine
			LR	RR,LR	[135,-135]	CW 180	[-45,45]	Fine

*Proceed as if LR(RR,RF,LF respectively) is the initial hit.

Table 2 Summary of control algorithm's actions corresponding to initial hits on sensors LF, RF, RR and LR.

FIGURE CAPTIONS

- Fig.1 Sketch of three vehicles to be aligned into an equilateral-triangle formation.
- Fig.2 Sketch of a cutaway section of the vehicle's air cavities.
- Fig.3 Geometry of the air-film bearing.
- Fig.4 Graphs of normalized pressure versus normalized radius for various values of p_1/p_a (computed values using Eq.(6): solid curves; linear approximation: dashed lines).
- Fig.5 (a) Sensor configuration; (b) Photograph of actual sensor module.
- Fig.6 Arrangement of six-jets for control.
- Fig.7 (a) Main flow chart for the rule-based control algorithm. (b) Flow charts for TAIL and FINE subroutines.
- Fig.8 Partitioning of angles for algorithm development.
- Fig.9 Control actions based on initial laser-beam hit on sensor.
- Fig.10 Vehicle motion sequence for a particular scenario.
- Fig.11 Computer simulation results showing the time-domain behavior of the Leader and Follower 1 during alignment for (a) the disturbance-free case; and (b) the case with 1-cm displacement perturbation along the x -direction introduced at $t = 31.75$ sec.
- Fig.12 Photograph of three air-levitated vehicles in an equilateral triangle formation.
- Fig.13 Computed (solid curve) and experimental points (+) of lower cavity air-pressure versus time.
- Fig.14 Coordinate system for vehicle simulation model (H denotes the vehicle front direction, and L the laser beam axis).
- Fig.15 Sketch of the cone C used for determining whether a sensor is hit by the laser beam.

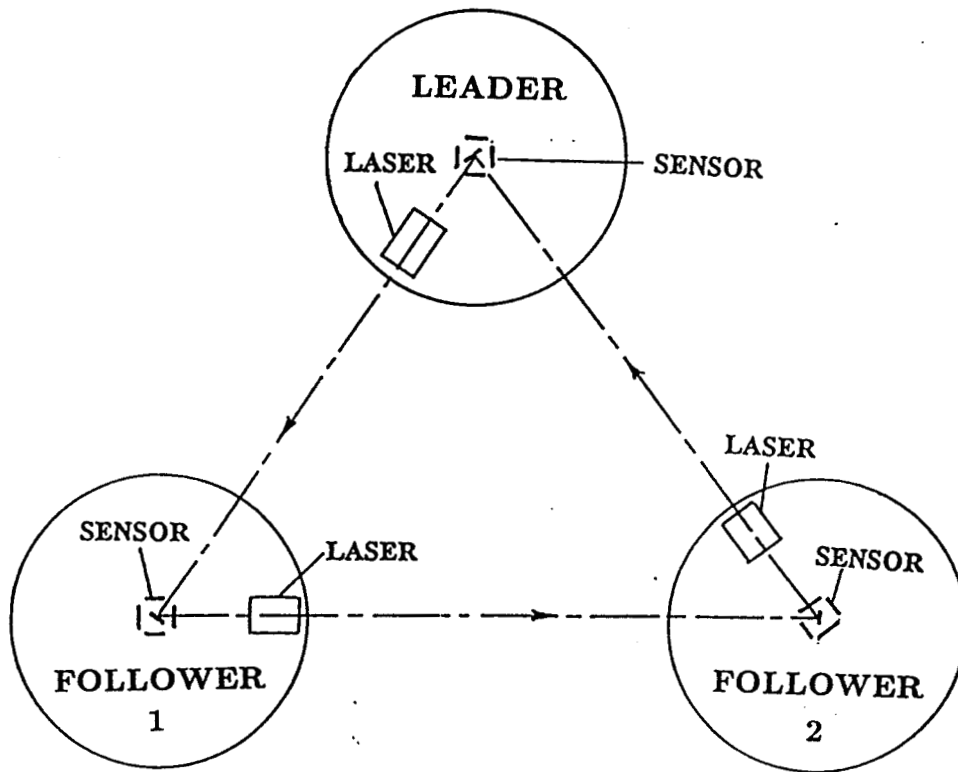


Fig. 1 Sketch of three vehicles to be aligned into an equilateral-triangle formation.

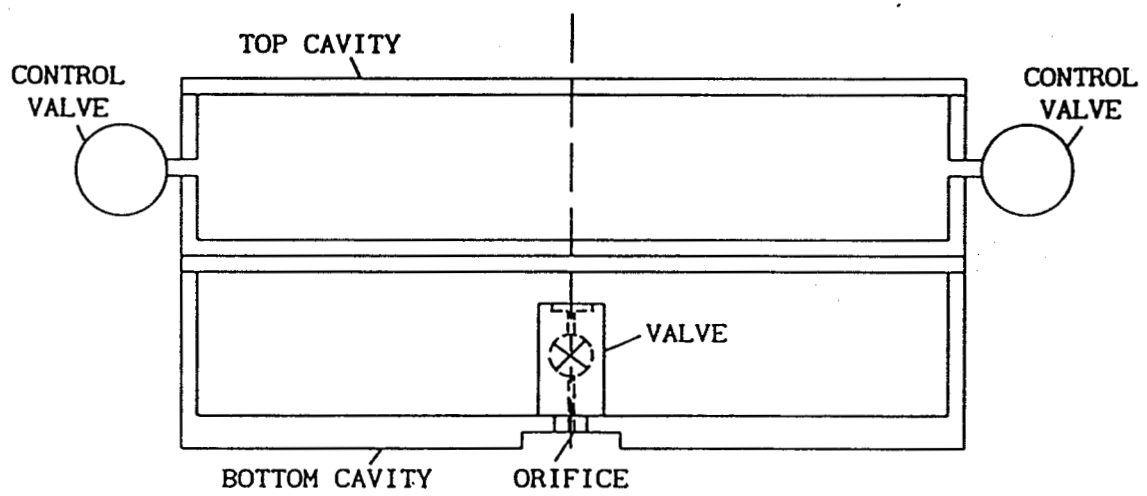


Fig.2 Sketch of a cutaway section of the vehicle's air cavities.

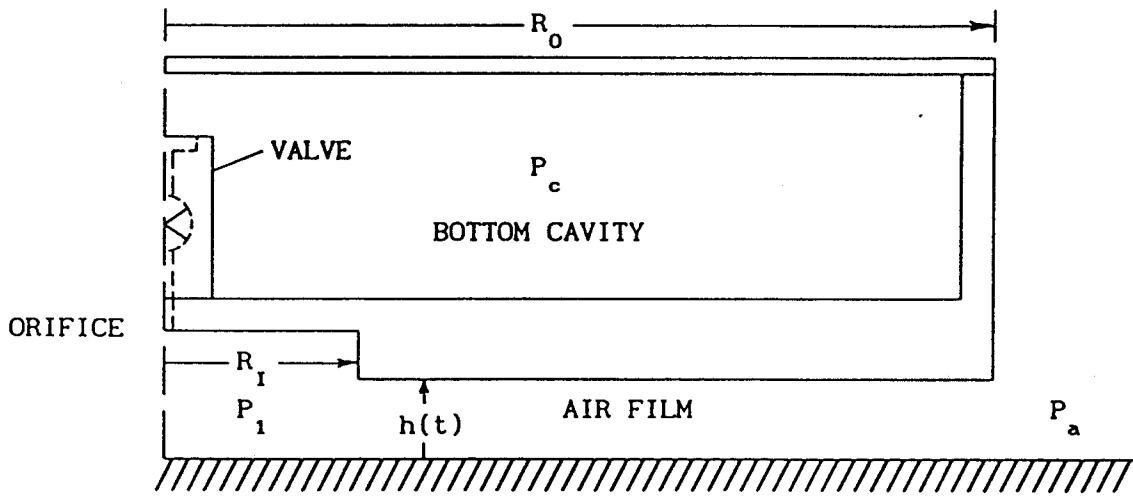


Fig.3 Geometry of the air-film bearing.

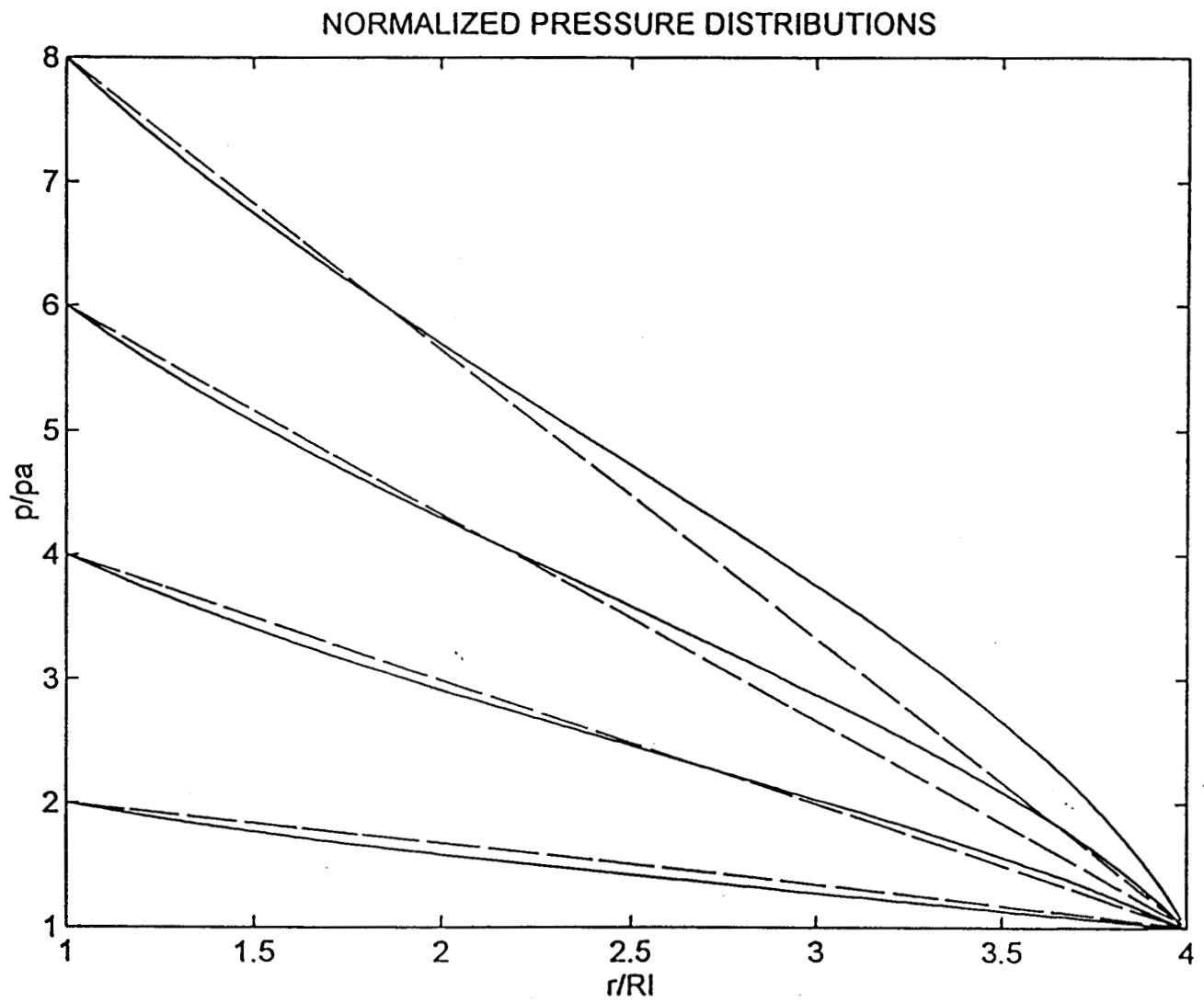
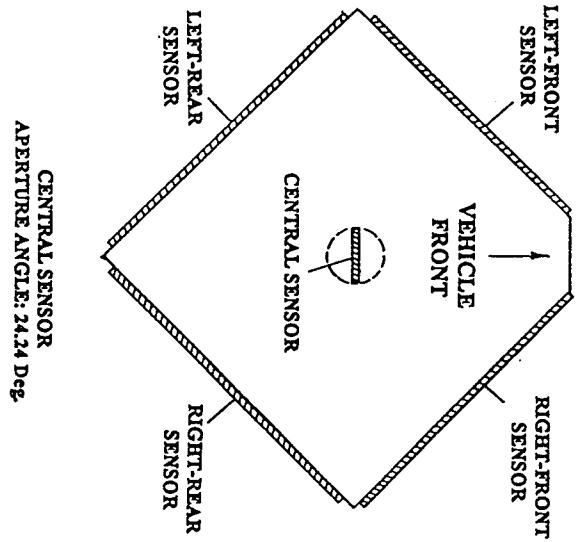
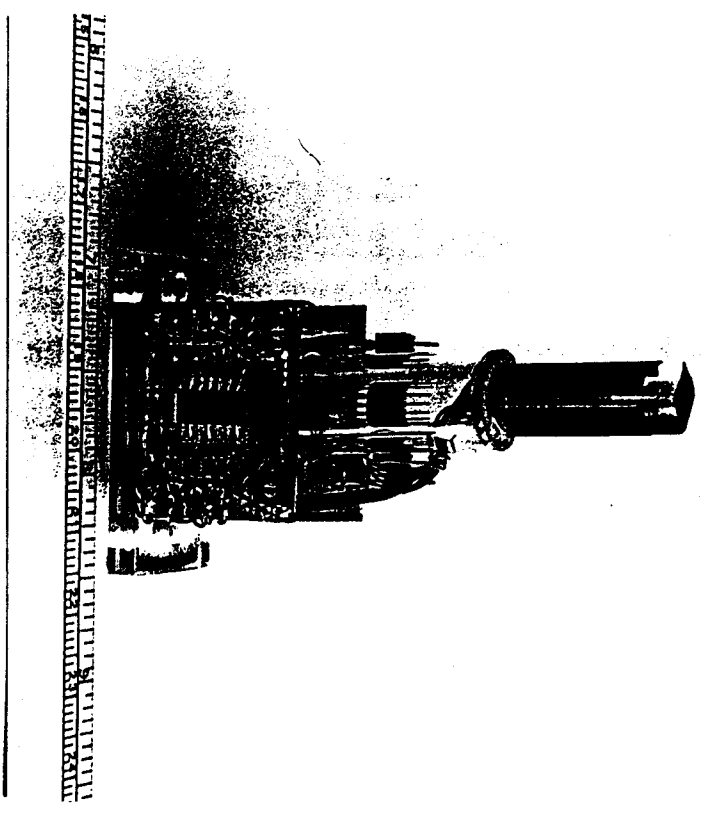


Fig.4 Graphs of normalized pressure versus normalized radius for various values of p_1/p_a (Computed values using Eq.(6): solid curves; linear approximation: dashed lines).



(a)



(b)

Fig.5 (a) Sensor configuration; (b) Photograph of actual sensor module.

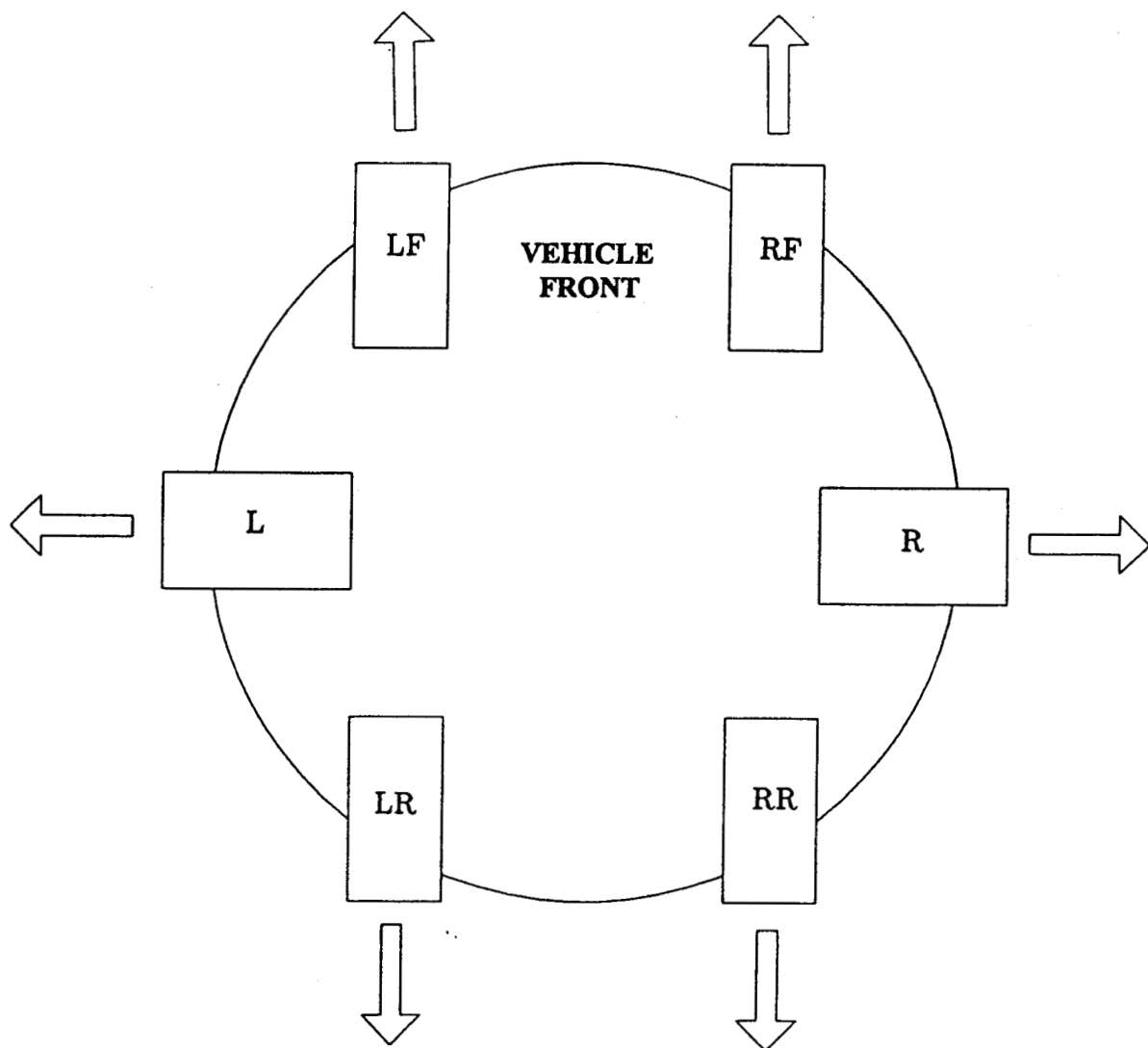


Fig.6 Arrangement of six air-jets for control.

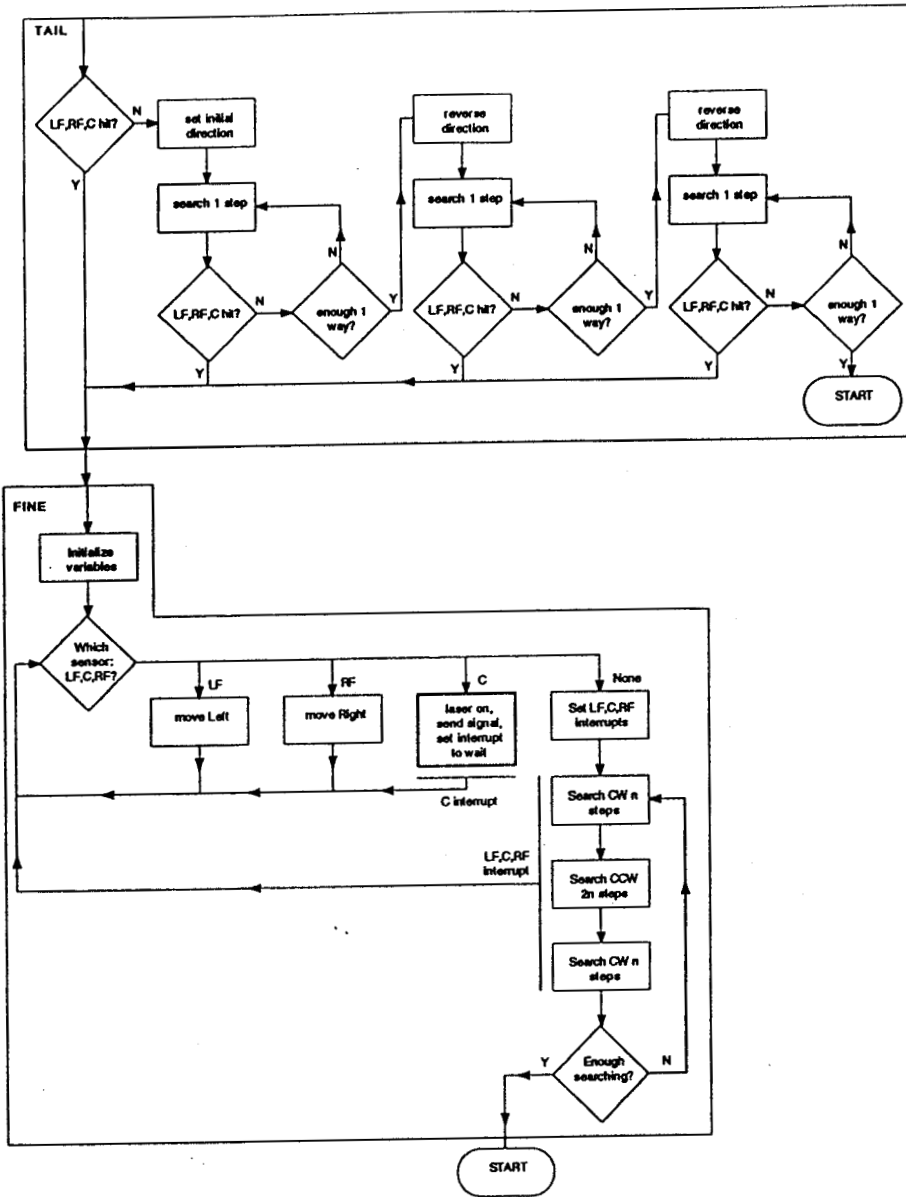


Fig.7 (b) Flow charts for TAIL and FINE subroutines.

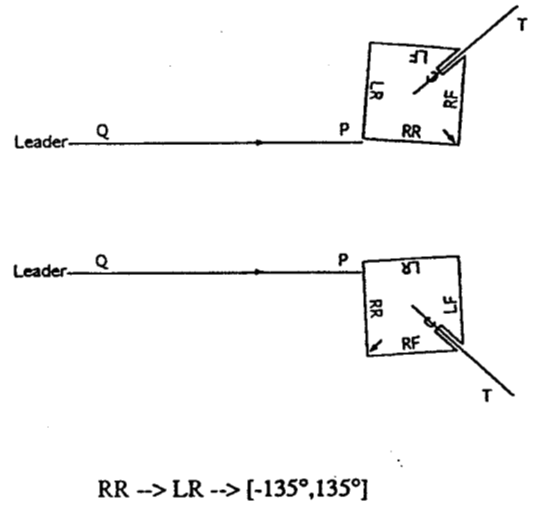
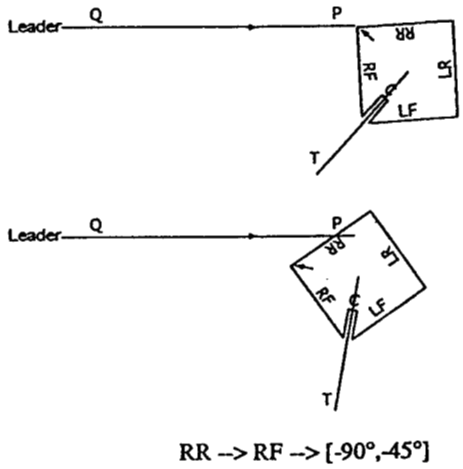
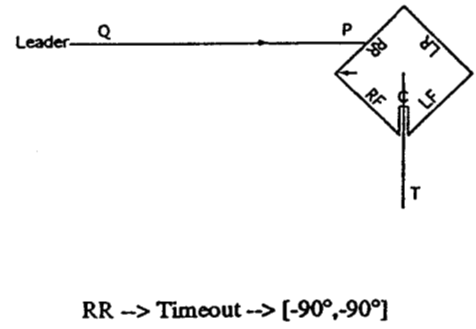
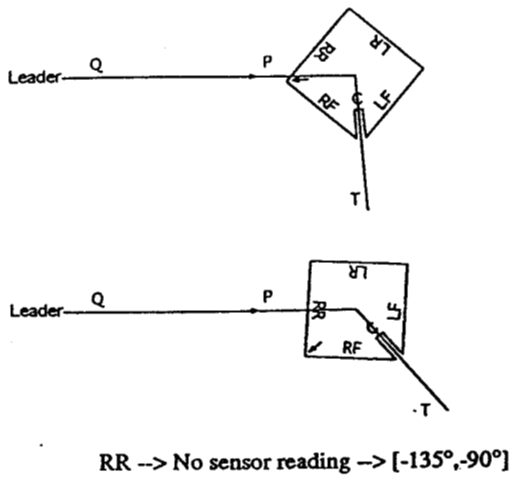


Fig.8 Partitioning of angles for algorithm development.

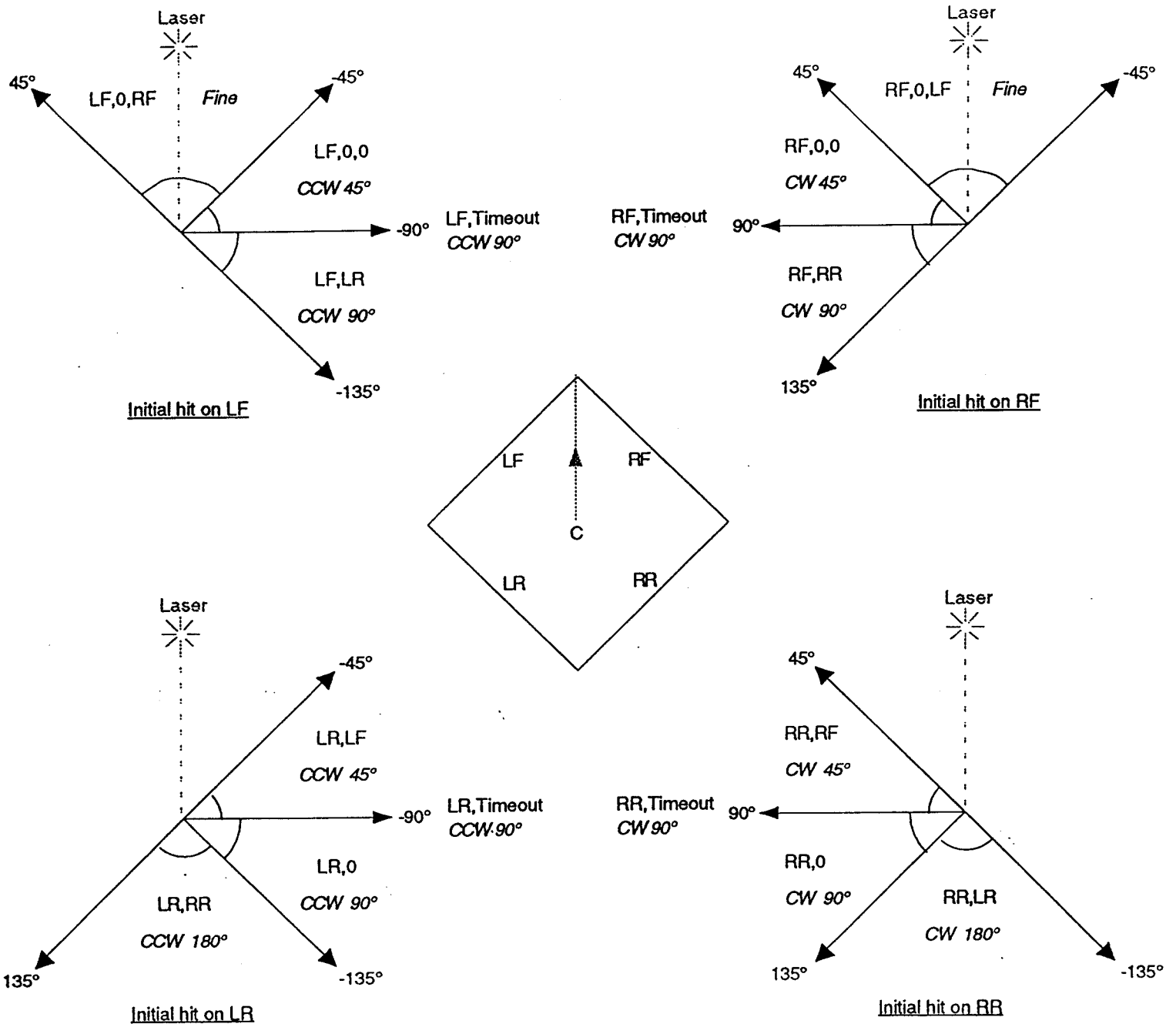


Fig.9 Control actions based on initial laser-beam hit on sensor.

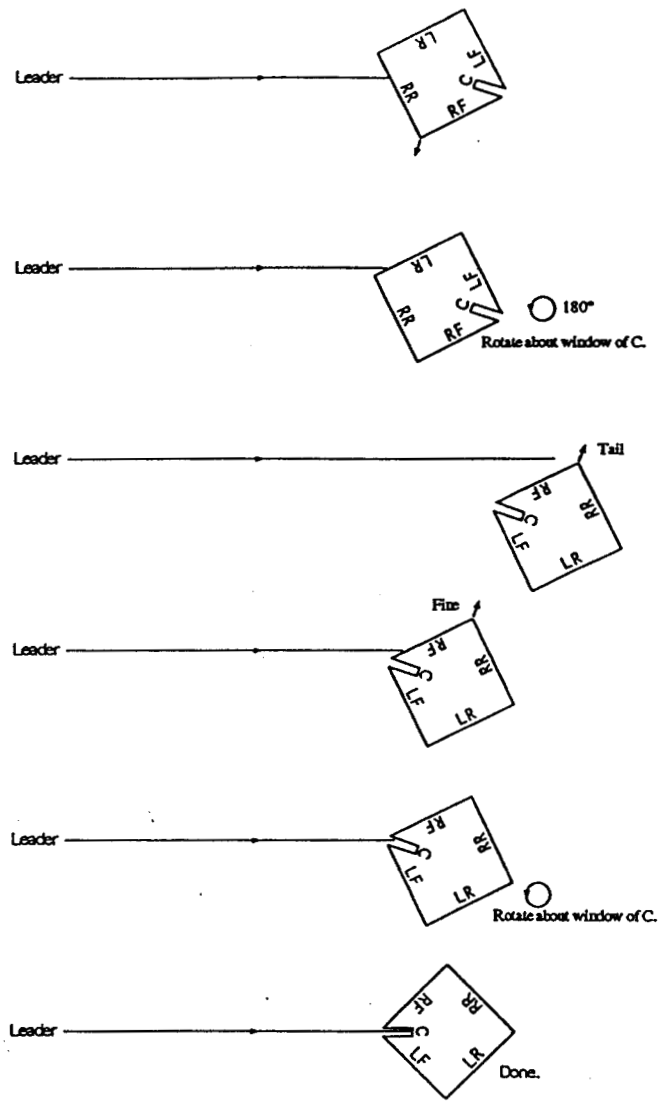


Fig.10 Vehicle motion sequence for a particular scenario.

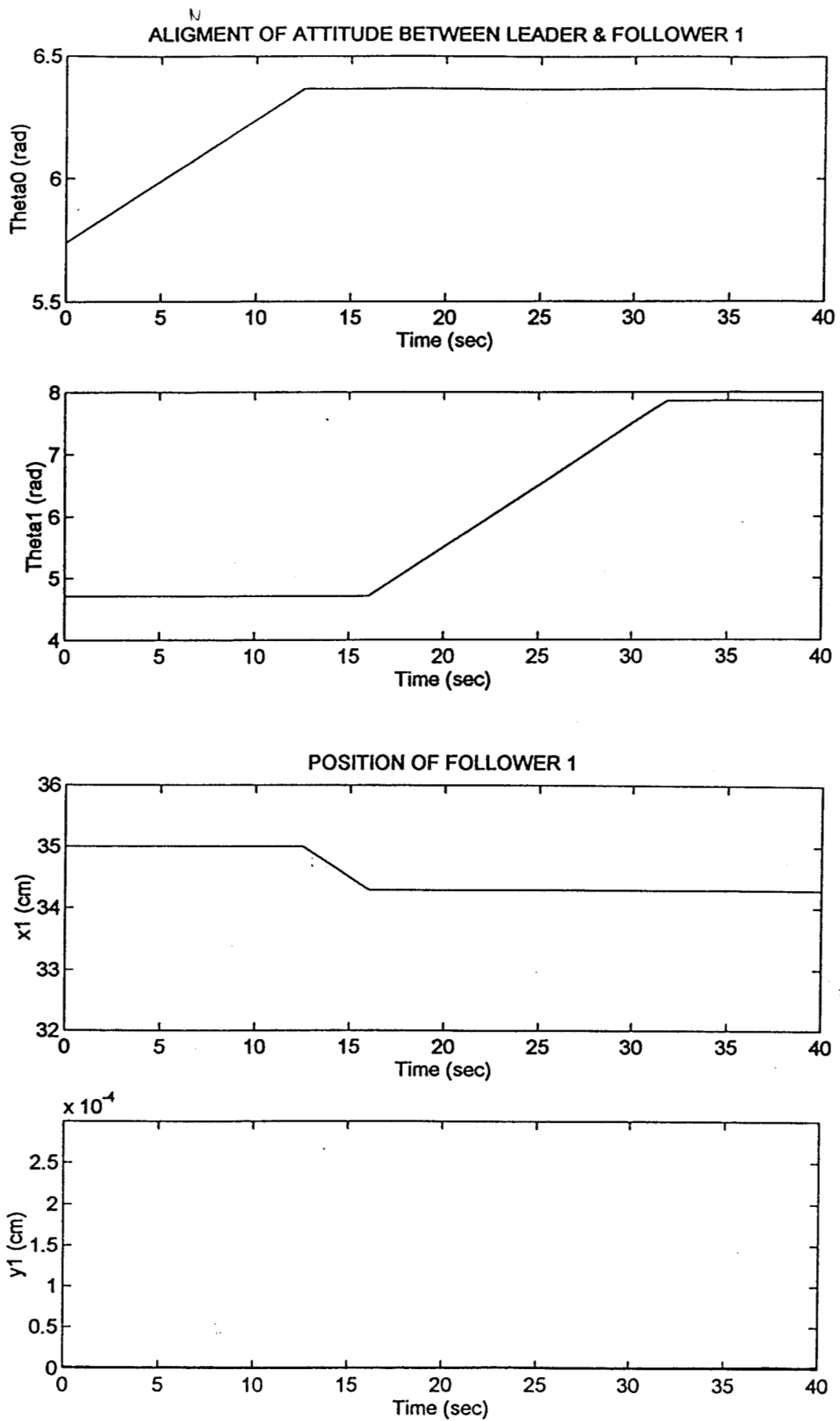


Fig.11 (a)

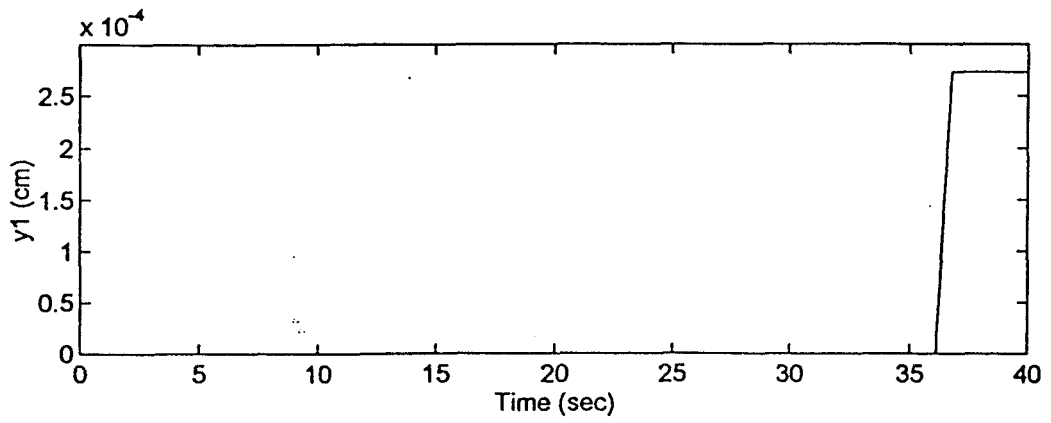
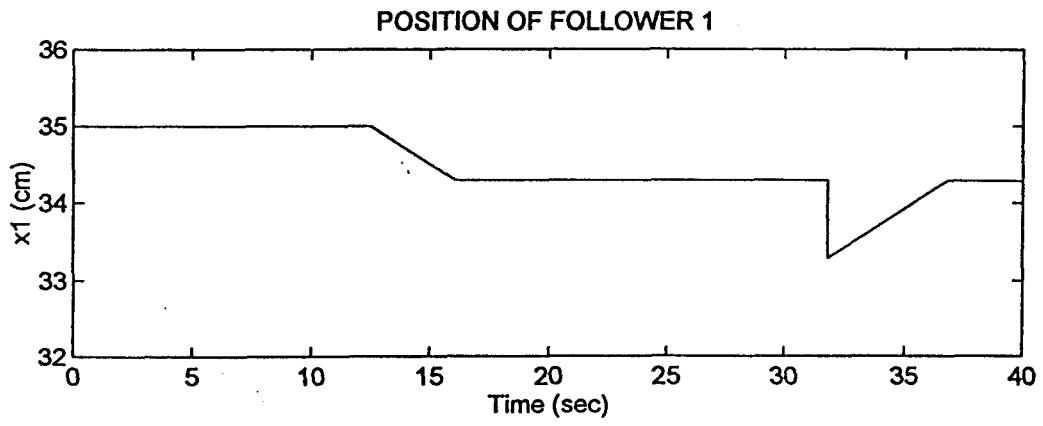
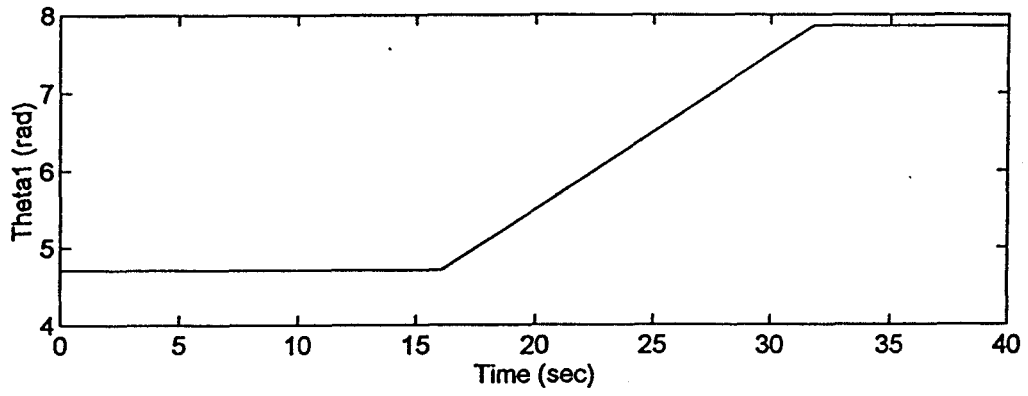
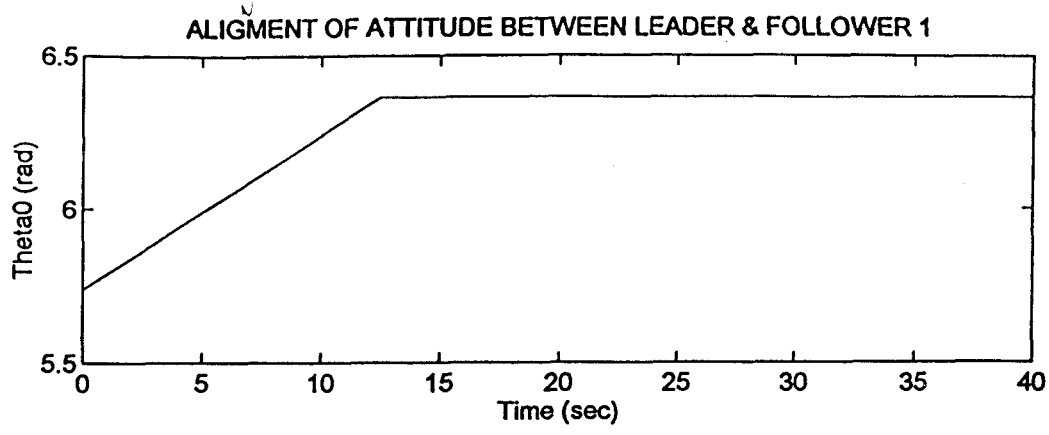


Fig.11 (b)

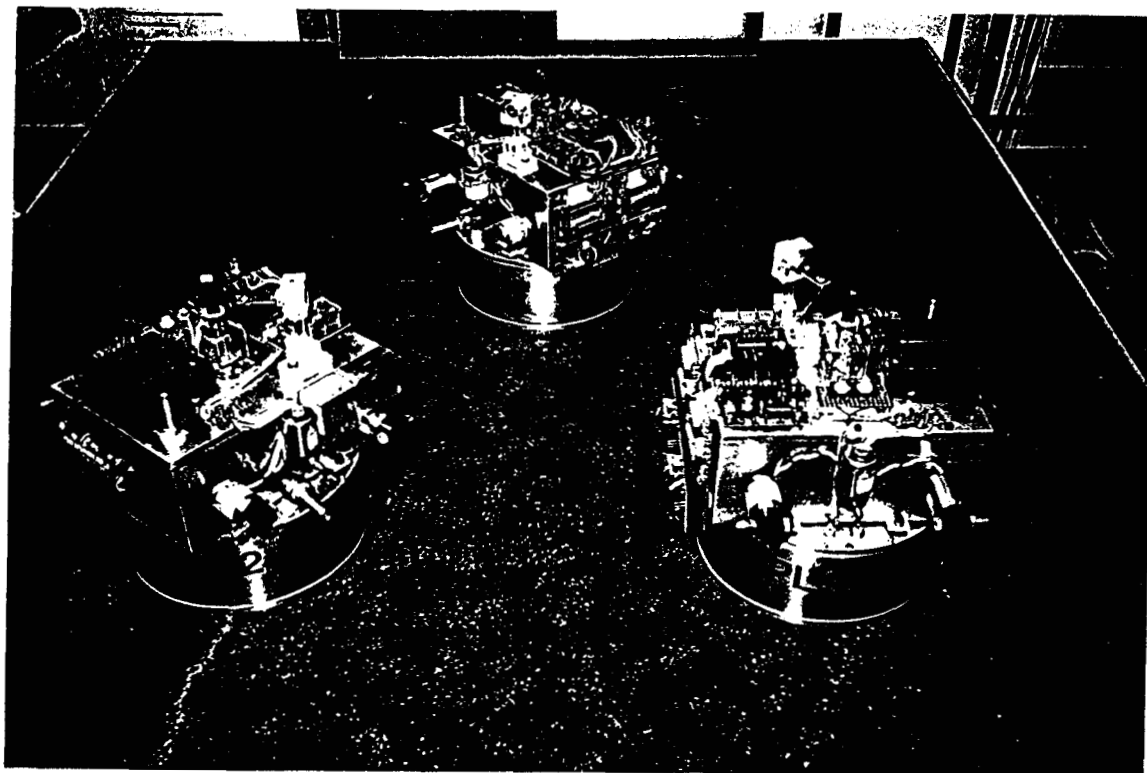


Fig.12 Photograph of three air-levitated vehicles in an equilateral triangle formation.

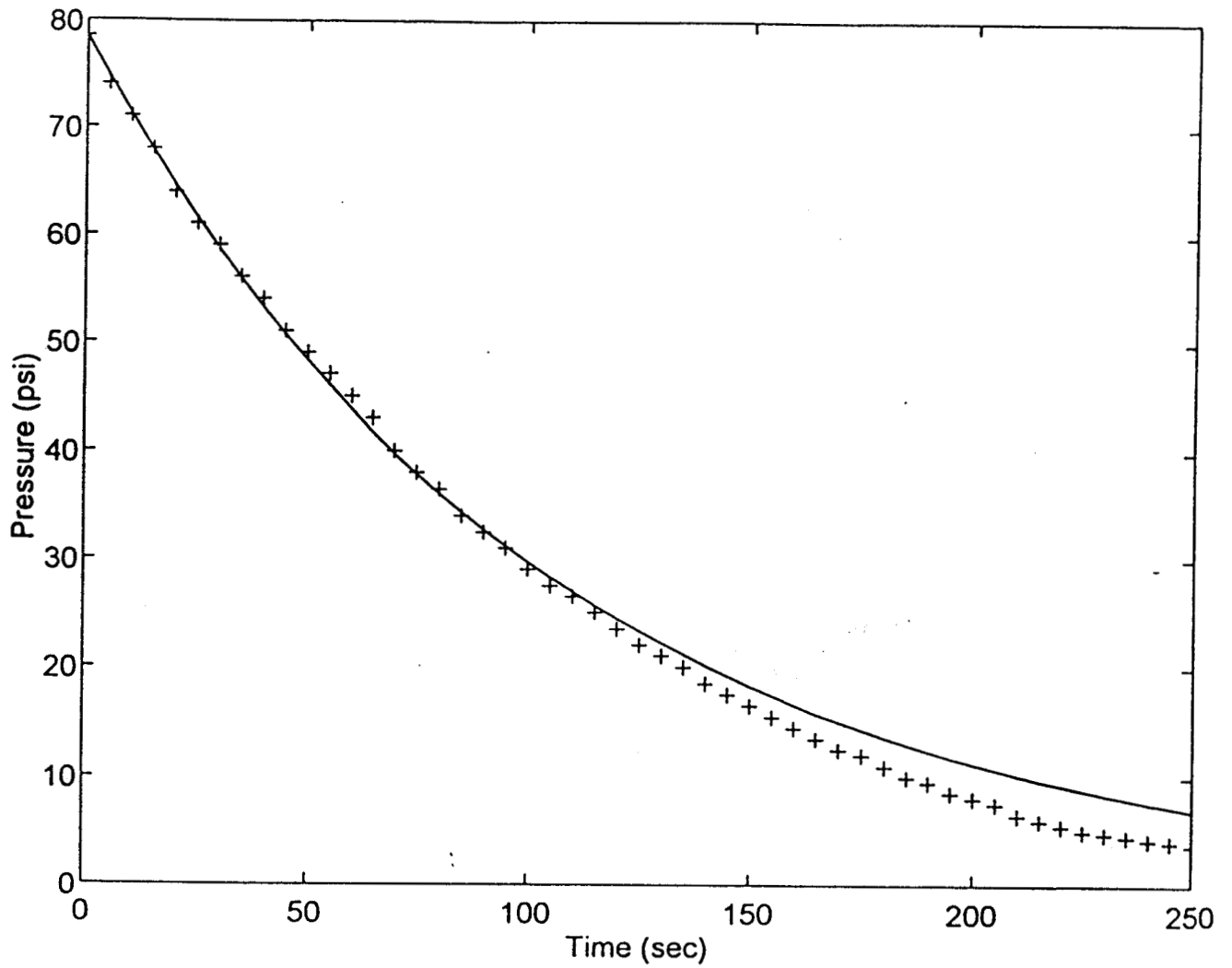


Fig.13 Computed (solid curve) and experimental points (+) of lower cavity air-pressure versus time.

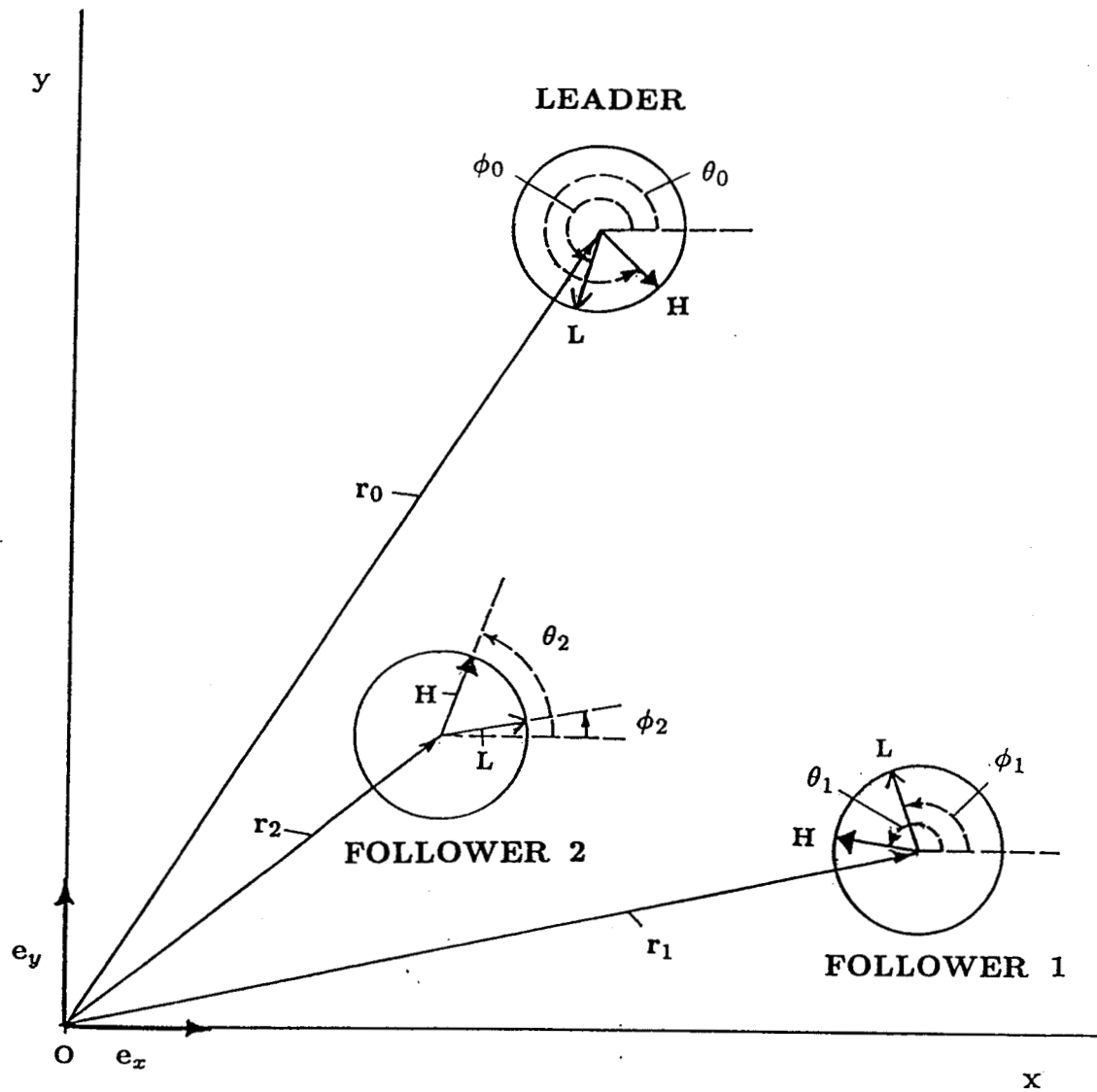


Fig.14 Coordinate system for vehicle simulation model (H denotes the vehicle front direction, and L the laser beam axis).

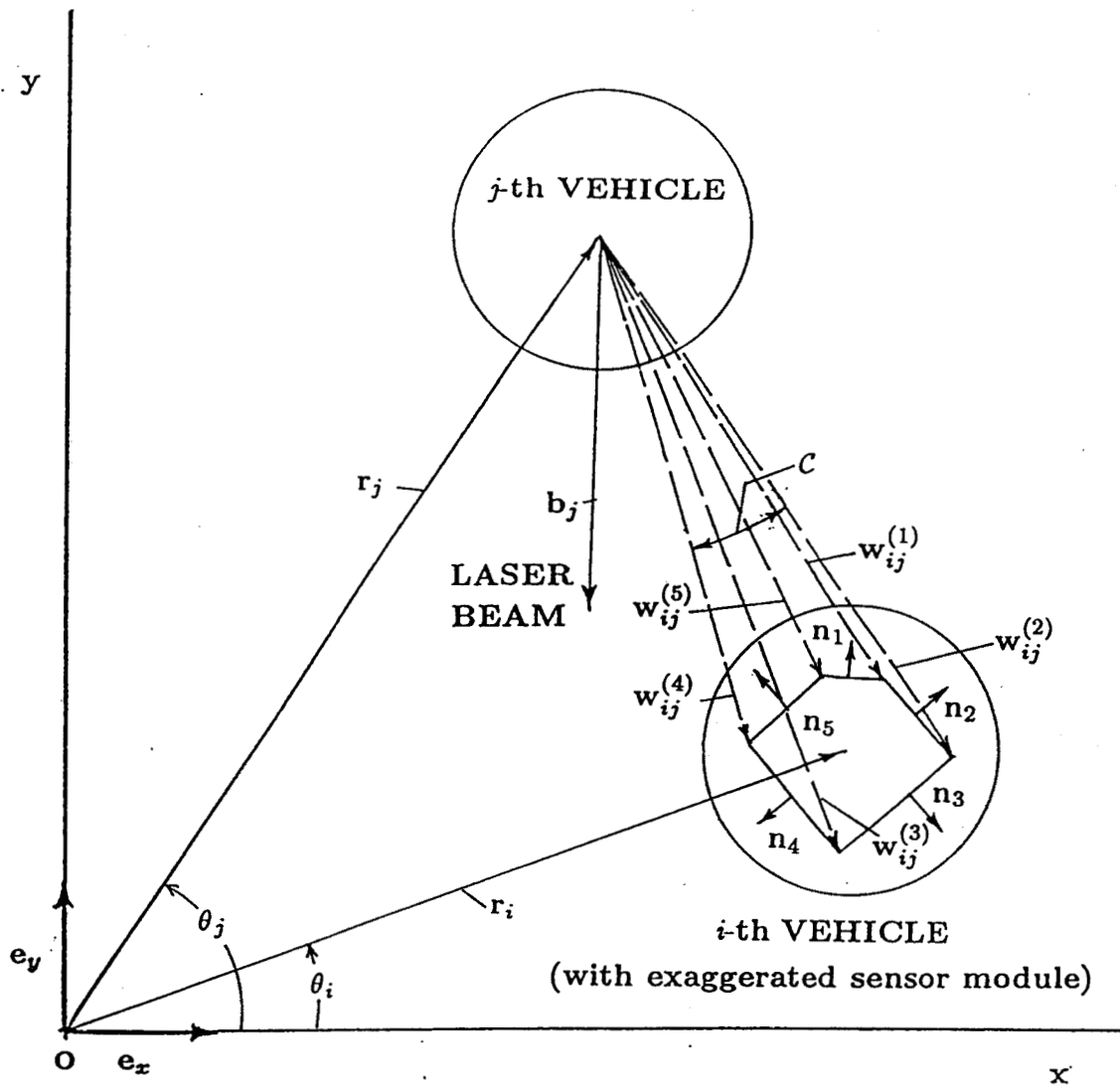


Fig.15 Sketch of the cone C used for determining whether a sensor is hit by the laser beam.